ISSN 1070-3284, Russian Journal of Coordination Chemistry, 2017, Vol. 43, No. 1, pp. 50–54. © Pleiades Publishing, Ltd., 2017.

Synthesis, Luminescent Sensing Based on a Three-Fold Interpenetrating Network with Flexible Carboxylates[1]

S. L. Cai*, T. Wang, J. Wang, B. Xie, and Y. Wu

School of Chemistry and Environmental Engineering, Sichuan University of Science and Engineering, Zigong, 643000 P.R. China

**e-mail: scwangjun2011@126.com*

Received December 17, 2016

Abstract—A Zn-based complexes with chemical formulae {[Zn(L)$_{0.5}$(4,4'-Bipy)] · 2H$_2$O} (**I**) (H$_4$L = 5,5'-(1,4-phenylene-bis(methylene))bis(oxy) diisophthalic acid), has been synthesized and structurally characterized. Single-crystal X-ray crystallography (CIF file CCDC no. 1465538) reveals that compound **I** shows a three-dimensional three-fold interpenetrating network simplified by a **bbf** topology (vertex symbol $(6^6)_2(6^4.8^2)$). Complex **I** can work as highly sensitive sensors to Cu^{2+}, CrO_4^{2-} and explosive by luminescent quenching.

Keywords: structure, topology, luminescent sensing

DOI: 10.1134/S107032841701002X

INTRODUCTION

Chemical sensors for fast and highly selective detection of high explosives and related substances have attracted increasing attention concerning homeland security, environmental and humanitarian implications [1–5]. Nowadays, some nanoscale materials (such as oligomeric, polymeric materials) are usually used for fluorescence detection. These materials are capable of quick and efficient detection of various explosives. However, there are still some hindrances, such as stability and sensitivity, thus it is a significant and challenging task to synthesize novel materials for fluorescence detection of explosives [6–11].

To date, scientists have developed all kinds of luminescent MOFs (LMOFs) sensors in various application fields [12–15] For example, Dinca's group has reported the Zn-based LMOFs which show high sensitivity to NH_3 [12]. Wang and his coworker have reported a new Zn-MOF that can reversibly detect H_2O by color conversion caused by hydration [13]. Chen and Qian synthesized a LMOF that can even function as the thermometer in the range of 10–300 K [14]. Furthermore, for the detection of metal ions with unsaturated electron configurations, new LMOF sensors keep emerging.

In this contribution we used H$_4$L to construct a new MOF of {[Zn(L)$_{0.5}$(4,4'-Bipy)] · 2H$_2$O} (**I**) (H$_4$L = 5,5'-(1,4-phenylenebis(methylene))bis(oxy) diisophthalic acid), which displays a three-dimensional three-fold interpenetrating network simplified by a **bbf** topology (vertex symbol $(6^6)_2(6^4.8^2)$). Complex **I** can work as highly sensitive sensors to Cu^{2+}, CrO_4^{2-} and explosive by luminescent quenching. Analyses of the structure indicate a higher quenching efficiency of **I** because of the existence of active COOH groups.

EXPERIMENTAL

Materials and methods. All reagents were purchased from commercial sources and used as received. IR spectra were recorded with a Perkin-Elmer Spectrum One spectrometer in the region 4000–400 cm^{-1} using KBr pellets. Termogravimetric analysis (TGA) was carried out with a Metter–Toledo TA 50 in dry dinitrogen (60 mL min^{-1}) at a heating rate of 5°C min^{-1}. X-ray powder diffraction (XRPD) data were recorded on a Rigaku RU200 diffractometer at 60 kV, 300 mA for CuK_α radiation (λ = 1.5406 Å), with a scan speed of 2°C/min and a step size of 0.013° in 2θ.

X-ray crystallography. Single crystal X-ray diffraction analysis of the title compound was carried out on a Bruker SMART APEX II CCD diffractometer equipped with a graphite monochromated MoK_α radiation (λ = 0.71073 Å) by using ϕ/ω scan technique at room temperature. Data were processed using the Bruker SAINT package and the structures solution and the refinement procedure was performed using SHELX-97 [16]. The structure was solved by direct methods and refined by full-matrix least-squares fit-

[1] The article is published in the original.

Table 1. Crystallographic data and structure refinement information for compound **I**

Parameter	Value
Crystal system	Monoclinic
Space group	$P2_1/n$
Crystal color	Colorless
a, Å	7.935(3)
b, Å	15.109(5)
c, Å	17.021(6)
β, deg	99.477(7)
V, Å^3	2012.8(12)
Z	4
ρ_{calcd}, g/cm^3	1.600
μ, mm^{-1}	1.270
F(000)	988
θ Range, deg	2.55–28.202
Reflection collected	12755
R_{int}	0.0872
Reflections with $I > 2\sigma(I)$	4840
Number of parameters	295
R_1, wR_2 ($I > 2\sigma(I)$)*	0.0735, 0.1716
R_1, wR_2 (all data)**	0.1743, 0.2208
$\Delta\rho_{max}$, $\Delta\rho_{min}$, e Å^{-3}	0.884/–0.732

* $R = \Sigma(F_o - F_c)/\Sigma(F_o)$, ** $wR_2 = \{\Sigma[w(F_o^2 - F_c^2)^2]/\Sigma(F_o^2)^2\}^{1/2}$.

Table 2. Selected bond distances (Å) and angles (deg) of structure **I**

Bond	d, Å	Angle	ω, deg
Zn(1)–O(1)	1.931(5)	O(1)Zn(1)O(3)	103.6(2)
Zn(1)–O(3)	1.937(4)	O(1)Zn(1)N(1)	135.9(2)
Zn(1)–N(1)	2.021(5)	O(3)Zn(1)N(1)	109.3(2)
Zn(1)–N(2)	2.074(5)		

ting on F^2. The hydrogen atoms of organic ligands were placed in calculated positions and refined using a riding on attached atoms with isotropic thermal parameters 1.2 times those of their carrier atoms. The lattice water molecule in compound **I** were not located due to their highly disordered. The details of the structure solutions and final refinements for complex are summarized in Table 1, selected bond distances/angles are listed in Table 2.

Syntheses of complex I. A mixture of $Zn(OAc)_2$ (0.021 g, 0.1 mmol), H_4L (0.012 g, 0.025 mmol), 4,4'-Bipy (0.014 g, 0.075 mmol), H_2O (3 mL), and CH_3CN (3 mL) was sealed in a Teflon-lined stainless steel vessel (25 mL), which was heated at 160°C for 3 days and then cooled to room temperature. Colorless block crystals of **I** were collected in 52% yield (0.0062 g, based on H_4L).

IR (KBr pellet; ν, cm^{-1}): 3455 v.s, 2835 m, 1599 v, 1539 v.s, 1450 v, 1339 v.s, 1238 m, 1120 v, 1055 v, 801 v.s, 718 v.s.

RESULTS AND DISCUSSION

Complex **I** features a 3D polymeric framework, which is similar with the compound reported in [17]. Each Zn atom is surrounded by two oxygen donors from two different L ligands and two N atoms from 4,4'-Bipy (Fig. 1), completing its tetrahedral coordination environment. All carboxyl groups of H_4L are deprotonated during the reaction and show monodentate mode to connect four Zn ions, and the side isophthalic rings and the central phenyl rings are nearly coplanar. The Zn ions were connected by L ligands to form 2D layers (Fig. 2), the dihedral angle between two adjacent coordinated phenyl rings is 87°.

The 4,4'-Bipy ligands bridge between pairs of metal atoms, while each L ligand, which lies across an inversion center, coordinates to four metal atoms. Topologically, the Zn atoms act as 4-connecting nodes, each connected to two other Zn nodes via the 4,4'-Bipy ligands, and to two L ligands. The L ligands in turn also act as 4-connecting nodes, with each connected to four Zn nodes; there are twice as many Zn nodes as L nodes. This generates an overall 3D network (Fig. 3) which has **bbf** topology (vertex symbol $(6^6)_2(6^4.8^2)$) [18].

As to FT–IR spectra, both the compounds show a broad band centered around 3400 cm^{-1} attributable to the O–H stretching frequency of the water cluster. The asymmetric stretching vibration ν(COO$^-$) appear around 1599 cm^{-1} and the symmetric stretching vibration ν(COO$^-$) are observed 1390 cm^{-1}. For the complex, the difference between the asymmetric and symmetric stretches, $\Delta\nu_{as}(COO^-) - \nu_s(COO^-)$, are on the order of 200 cm^{-1} indicating that carboxyl groups are coordinated to the metal in a monodentate modes [19], consistent with the observed X-ray crystal structure of **I**.

To study the stability of complex **I** TGA was carried out. The TG diagram of **I** shows two weight loss steps. The first weight loss began at 35°C and completed at 158°C. The observed weight loss of 7.1% is corresponding to the loss of the lattice water molecules (calcd. 6.9%). The second weight loss occurs in the range 390–810°C, which can be attributed to the elimination of L and Bipy ligands.

Additionally, to confirm the phase purity and stability of compound **I**, both the original samples were characterized by XRPD. Although the experimental patterns have a few unindexed diffractions lines and some are slightly broadened in comparison to those

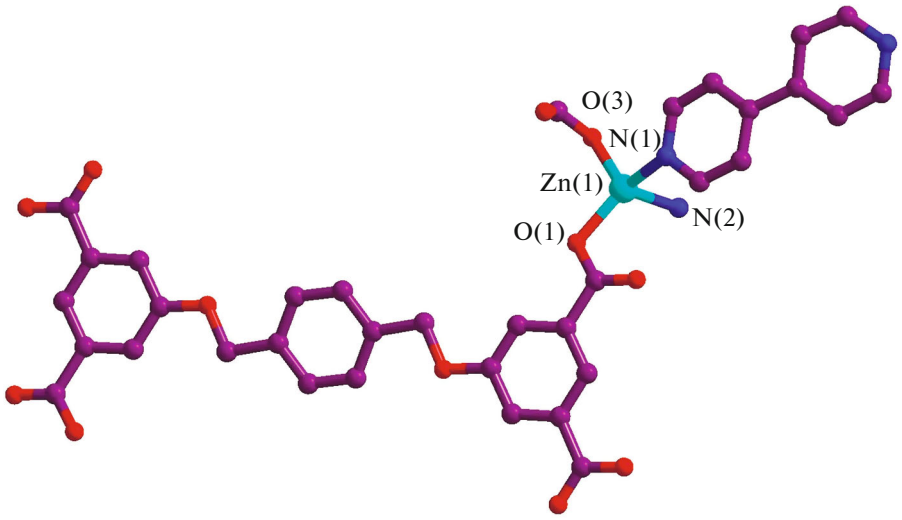

Fig. 1. The coordination geometries of the metal centers and the ligands geometries in **I**. Displacement ellipsoids are drawn at the 30% probability level and H atoms are omitted for clarity.

simulated from single-crystal models, it can still to be considered that the bulk synthesized materials and as-grown crystal are homogeneous for compound **I**.

The photoluminescence (PL) spectra of **I** and H_4L in the solid state were recorded at room temperature. Compound **I** exhibited an emission peak at 470 nm upon excitation at 370 nm. This emission band can be assigned to H_4L ligand-centered emission, because similar emission was observed at 366 nm (λ_{ex} = 300 nm) for the free H_4L ligand [17]. In addition, the fluorescence properties of **I** in different solvent emulsions were investigated (Figs. 4a, 4b). The predominant feature is that the PL intensities are largely dependent on the solvent molecules, particularly in the case of nitrobenzene (NB), which exhibits significant quenching behavior [20]. The physical interaction of the solute and solvent plays a vital role in such fluorescence behavior [21]. To examine sensing sensitivity towards NB in more detail, a batch of suspensions of **I** with gradually increasing NB contents in DMF was prepared to monitor the emissive response (Fig. 4c). The luminescence intensity decreased to 50% at 330 ppm, and almost complete quenching was

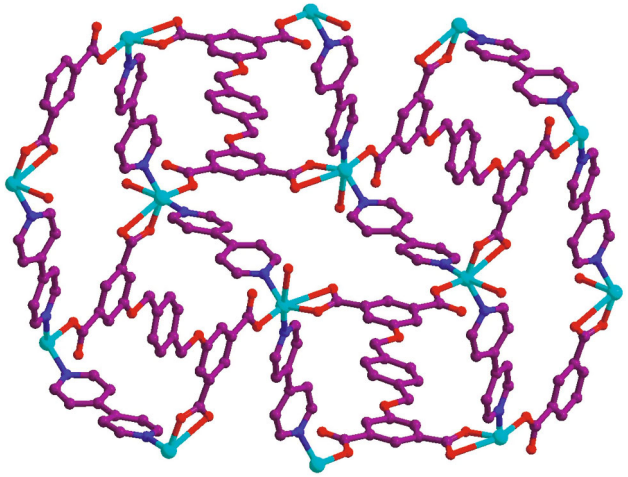

Fig. 2. View of the 3D packing framework.

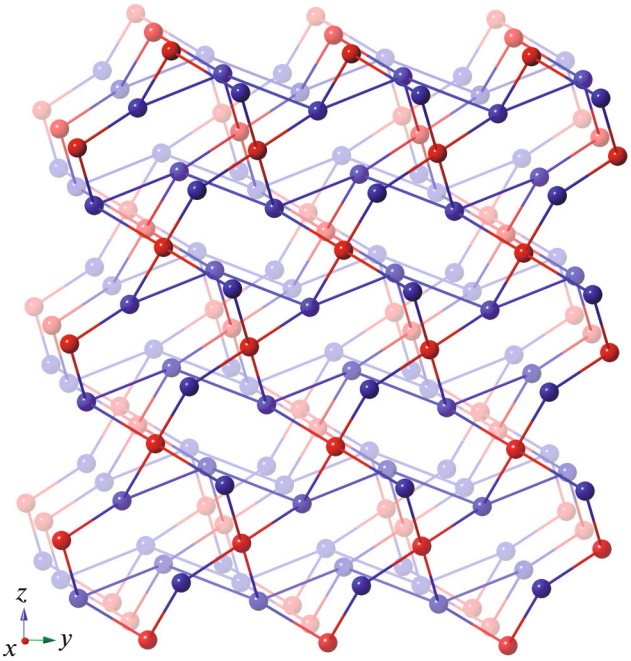

Fig. 3. The underlying **bbf** net in **I**. Blue spheres represent Zn nodes, while red spheres represent the L ligands.

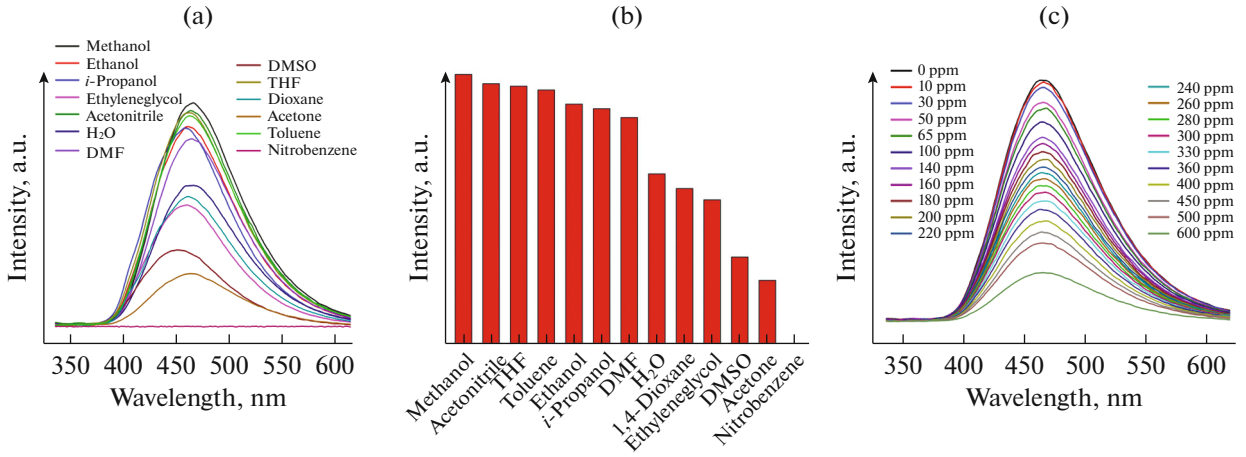

Fig. 4. Comparison of the relative luminescence intensities of various **I**/solvents in DMF suspensions (a) and (b); emission spectra of **I** dispersed in DMF with the titration of NB (c).

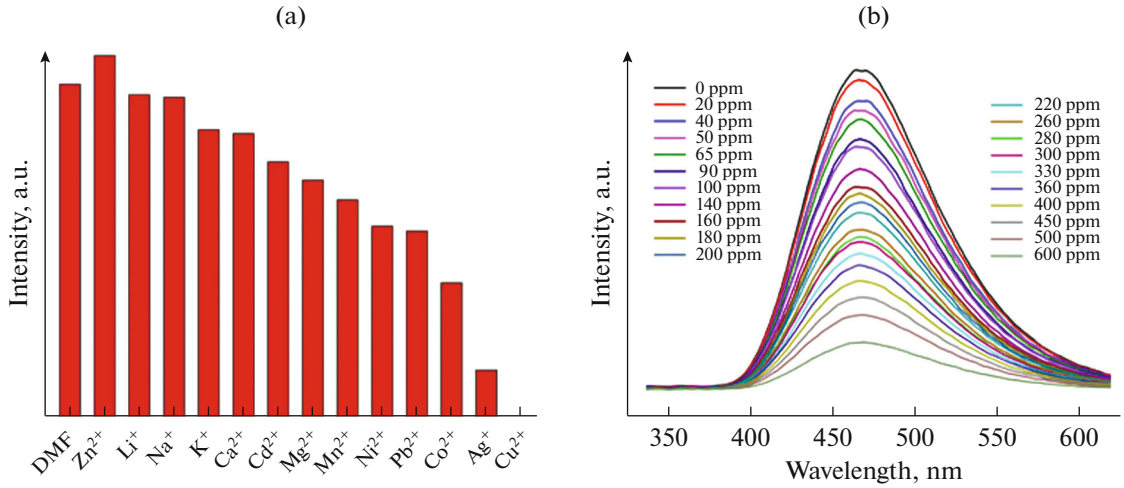

Fig. 5. Comparison of the relative luminescence intensities of various **I**/metal ions in DMF suspensions (a); emission spectra of **I** dispersed in DMF with the titration of Cu^{2+} (b).

received at 600 ppm. Therefore, this results indicate that electron transfer from the electron-donating framework to the highly electron-deficient NB molecule can take place upon excitation, resulting in fluorescence quenching [22–25].

The luminescence spectra of **I** (3 mg) dispersed in DMF solutions (5 mL) of metal ions 5 mg, $NaNO_3$, KNO_3, $LiNO_3$, $Ca(NO_3)_2$, $Zn(NO_3)_2$, $Cd(NO_3)_2$, $Pb(NO_3)_2$, $Ni(NO_3)_2$, $Cu(NO_3)_2$, $Mn(NO_3)_2$, $Co(NO_3)_2$, and $Mg(NO_3)_2$ are studied. Figure 5a clearly clarifies that metal ions with saturated electron configurations cannot cause a significant change to the luminescent intensity; in contrast, the other reduction, especially for Cu^{2+}, can bring essentially complete quenching to the system. This result demonstrates that compound of **I** can be highly effective and selective luminescent sensors for Cu^{2+} ions. The decreases of intensity caused by Cu^{2+} ions induce LMCT and provide a non-radiative pathway for the excitation energy [26–28].

The quenching effect of Cu^{2+} ion the luminescence intensity of **I** has been further examined (Fig. 5b). The quenching effect can be quantitatively explained by the Stern–Volmer equation [29]

$$I_0/I = 1 + K_{SV}[M],$$

I_0 and I are the luminescent intensity before and after metal ion incorporation, respectively. [M] is the metal ion molar concentration. K_{SV} is the coefficient of quenching. The reduction of luminescent intensity is proportional to metal ion concentration. The K_{SV} can be calculated via luminescent data. The Cu^{2+} has the most significant effect on the luminescence quenching of **I** with the largest K_{SV} of 8083.3 M^{-1}. Such highly

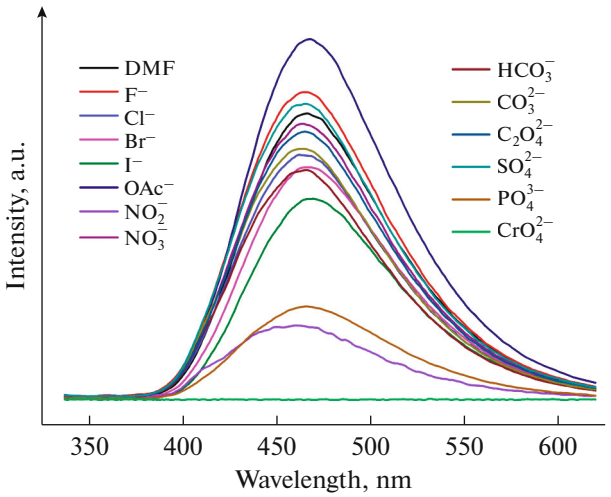

Fig. 6. Comparison of the relative luminescence intensities of various **I**/anions in DMF suspensions.

selective and sensitive sensing of Cu^{2+} in aqueous solution is really remarkable. The confined small pores within **I** enhance the recognition of Cu^{2+} ions through the binding among the Cu^{2+} ions and the uncoordinated carboxylate sites on the pore surfaces, leading to a much more sensitive and selective microporous LMOF sensor [30].

To further examine the potential luminescence sensing properties of **I** for anions, the fine grinding samples **I** was immersed in different DMF solutions (5 mL) of anions. The most interesting feature is that the luminescence intensity of the anion incorporated **I** is heavily metal ion dependent: X^- anion and almost anions have basically no effect on the luminescence intensity, while others have different degrees of quenching effects on the luminescence intensity with the CrO_4^{2-} the most significant (Fig. 6) [31].

ACKNOWLEDGMENTS

The authors thanks prof. S.R. Batten for structural analysis of topology.

The authors acknowledge financial assistance from Sichuan University of Science and Engineering (nos. 2014PY01, 2015PY03, 2014RC34, and 2015RC26), and the Education Committee of Sichuan Province (nos. 14ZB0212, 14ZB0220, 15ZB0222, 15ZB0214).

REFERENCES

1. Shekhah, O., Liu, J., Fischer, R.A., and Woll, C., *Chem. Soc. Rev.*, 2011, vol. 40, p. 1081.
2. Chen, B., Wang, L.B., Xiao, Y.Q., et al., *Angew. Chem. Int. Ed.*, 2009, vol. 48, p. 500.
3. Kreno, L.E., Leong, K., Farha, O.K., et al., *Chem. Rev.*, 2012, vol. 112, p. 1105.
4. Liu, J.Q., Wu, J., Li, F.M., et al., *RSC Adv.*, 2016, vol. 6, p. 31161.
5. Hu, Z.C., Deibert, B.J., and Li, J., *Chem. Soc. Rev.*, 2014, vol. 43, p. 5815.
6. Jin, J.C., Pang, L.Y., Yang, G.P., et al., *Dalton Trans.*, 2015, vol. 44, p. 17222.
7. Li, B.H., Wu, J., Liu, J.Q., et al., *ChemPlusChem*, 2016, vol. 81, p. 885.
8. Hao, Z.M., Song, X.Z., Zhu, M., et al., *J. Mater. Chem. A*, 2013, vol. 1, p. 11043.
9. Chen, B., Wang, L.B., Xiao, Y.Q., et al., *Angew. Chem., Int. Ed.*, 2009, vol. 48, p. 500.
10. Liu, B., Wu, W.P., Hou, L., and Wang, Y.Y., *Chem. Commun.*, 2014, vol. 50, p. 8731.
11. Chen, B., Zhao, X., Putkham, A., et al., *J. Am. Chem. Soc.*, 2008, vol. 130, p. 6411.
12. Shustova, N.B., Cozzolino, A.F., Reineke, S., et al., *J. Am. Chem. Soc.*, 2013, vol. 135, p. 13326.
13. Wang, C.C., Yang, C.C., Chung, W.C., et al., *Chem. Eur. J.*, 2011, vol. 17, p. 9232.
14. Cui, Y., Xu, H., Yue, Y., et al., *J. Am. Chem. Soc.*, 2012, vol. 134, p. 3979.
15. Chen, B., Yang, Y., Zapata, F., et al., *Adv. Mater.*, 2007, vol. 19, p. 1693.
16. Sheldrick, G. M., *SHELXTL, Version 5.1, Software Reference Manual*, Madison (WI, USA): Bruker AXS, Inc., 1997.
17. He, X., Lu, X.P.Z., Ju, F., et al., *CrystEngComm*, 2013, vol. 15, p. 2731.
18. O'Keeffe, M., Peskov, M.A., Ramsden, S., and Yaghi, O.M., *Acc. Chem. Res.*, 2008, vol. 41, p. 1782.
19. Nakamoto, K., *Infrared and Raman Spectra of Inorganic and Coordination Compounds*, New York: Wiley Interscience, 1997.
20. Germain, M.E. and Knapp, M.J., *Chem. Soc. Rev.*, 2009, vol. 38, p. 2543.
21. Jiang, H.L., Feng, D.W., Wang, K.C., et al., *J. Am. Chem. Soc.*, 2013, vol. 135, p. 13934.
22. Yin, Z., Wang, Q.X., and Zeng, M.H., *J. Am. Chem. Soc.*, 2012, vol. 134, p. 4857.
23. Chaudhari, A.K., Nagarkar, S.S., Joarder, B., and Ghosh, S.K., *Cryst. Growth Des.*, 2013, vol. 13, p. 3716.
24. Nielsen, K.A., Cho, W.S., Jeppesen, J.O., et al., *J. Am. Chem. Soc.*, 2004, vol. 126, p. 16296.
25. Park, J.S., Derf, F.L., Bejger, C.M., et al., *Chem.-Eur. J.*, 2010, vol. 16, p. 848.
26. Hu, Z.C., Deibert, B.J., and Li, J., *Chem. Soc. Rev.*, 2014, vol. 43, p. 5815.
27. Wang, Y., Yang, J., Liu, Y.-Y., and Ma, J.-F., *Chem. Eur. J.*, 2013, vol. 19, p. 14591.
28. Cui, Y., Yue, Y., Qian, G., and Chen, B., *Chem. Rev.*, 2012, vol. 112, p. 1126.
29. Gole, B., Bar, A.K., and Mukherjee, P.S., *Chem. Eur. J.*, 2014, vol. 20, p. 2276.
30. Chen, B., Xiang, S., and Qian, G., *Acc. Chem. Res.*, 2010, vol. 43, p. 1115.
31. Liu, C. and Yan, B., *Photochem. Photobiol. Sci.*, 2015, vol. 14, p. 1644.